The Impact of Interacting Climate Modes on East Australian Precipitation Moisture Sources

CHIARA HOLGATE,[a,b] JASON P. EVANS,[b,c] ANDRÉA S. TASCHETTO,[b,c] ALEX SEN GUPTA,[b,c] AND AGUS SANTOSO[b,c,d]

[a] *Fenner School of Environment and Society, Australian National University, Canberra, Australia*
[b] *ARC Centre of Excellence for Climate Extremes, University of New South Wales, Sydney, Australia*
[c] *Climate Change Research Centre, University of New South Wales, Sydney, Australia*
[d] *Centre for Southern Hemisphere Oceans Research, CSIRO Oceans and Atmosphere, Hobart, Australia*

(Manuscript received 29 September 2021, in final form 22 January 2022)

ABSTRACT: Modes of climate variability can drive significant changes to regional climate affecting extremes such as droughts, floods, and bushfires. The need to forecast these extremes and expected future increases in their intensity and frequency motivates a need to better understand the physical processes that connect climate modes to regional precipitation. Focusing on east Australia, where precipitation is driven by multiple interacting climate modes, this study provides a new perspective into the links between large-scale modes of climate variability and precipitation. Using a Lagrangian back-trajectory approach, we examine how El Niño–Southern Oscillation (ENSO) modifies the supply of evaporative moisture for precipitation, and how this is modulated by the Indian Ocean dipole (IOD) and southern annular mode (SAM). We demonstrate that La Niña modifies large-scale moisture transport together with local thermodynamic changes to facilitate local precipitation generation, whereas below-average precipitation during El Niño stems predominantly from increased regional subsidence. These dynamic–thermodynamic processes were often more pronounced during co-occurring La Niña/negative IOD and El Niño/positive IOD periods. As the SAM is less strongly correlated with ENSO, the impact of co-occurring ENSO and SAM largely depended on the state of ENSO. La Niña–related processes were exacerbated when combined with +SAM and dampened when combined with −SAM, and vice versa during El Niño. This new perspective on how interacting climate modes physically influence regional precipitation can help elucidate how model biases affect the simulation of Australian climate, facilitating model improvement and understanding of regional impacts from long-term changes in these modes.

SIGNIFICANCE STATEMENT: How climate modes modulate the oceanic and terrestrial sources of moisture for rainfall in east Australia is investigated. East Australia is wetter during La Niña because more moisture is transported into the region and is more easily turned into rainfall when it arrives, whereas drier conditions during El Niño are because local conditions inhibit the conversion of moisture into rainfall. Distant atmospheric changes over the Indian and Southern Oceans can intensify these changes. Our results can be used to better understand and predict the regional impact of long-term changes in these modes of climate variability, which are potentially altered under climate change.

KEYWORDS: ENSO; Lagrangian circulation/transport; Teleconnections; Precipitation; Water vapor

1. Introduction

Modes of climate variability have a pronounced impact on global and regional climate with important socioeconomic consequences (Glantz 2001; Iizumi et al. 2014; McPhaden et al. 2006). Across Australia multiple modes of climate variability interact to modulate precipitation (Ashok et al. 2003a; Hendon et al. 2007; Pui et al. 2012; Risbey et al. 2009) and temperature (Arblaster and Alexander 2012; Jones and Trewin 2000; Saji et al. 2005), affecting the likelihood of climate extremes such as bushfires, droughts, floods, and heat waves (Abram et al. 2021; Cai et al. 2009; Chiew et al. 1998; Evans and Boyer-Souchet 2012; Perkins et al. 2015; Ummenhofer et al. 2009, 2010, 2015). Precipitation in east Australia, in particular, is associated with El Niño–Southern Oscillation (ENSO; e.g., van Rensch et al. 2019; Chiew et al. 1998), the Indian Ocean dipole (IOD; e.g., Ashok et al. 2003a), and the southern annular mode (SAM; e.g., Hendon et al. 2007).

The warm phase of ENSO, El Niño, is often associated with drier conditions in east Australia (Cai et al. 2011b; Risbey et al. 2009) primarily resulting from fewer wet spells (Pui et al. 2012). During an El Niño event, anomalous warming of the central-to-eastern tropical Pacific Ocean typically starts to occur in austral winter and peaks in summer, weakening the Walker circulation and trade winds (Santoso et al. 2017). In association, cooler-than-normal sea surface temperatures (SSTs) tend to occur north of Australia that lead to large-scale subsidence and higher surface pressure in the

Supplemental information related to this paper is available at the Journals Online website: https://doi.org/10.1175/JCLI-D-21-0750.s1.

Chiara Holgate's current affiliation: Research School of Earth Sciences, Australian National University, Canberra, Australia.

Corresponding author: Chiara Holgate, chiara.holgate@anu.edu.au

DOI: 10.1175/JCLI-D-21-0750.1

© 2022 American Meteorological Society. For information regarding reuse of this content and general copyright information, consult the AMS Copyright Policy (www.ametsoc.org/PUBSReuseLicenses).

Unauthenticated | Downloaded 01/24/24 02:40 AM UTC

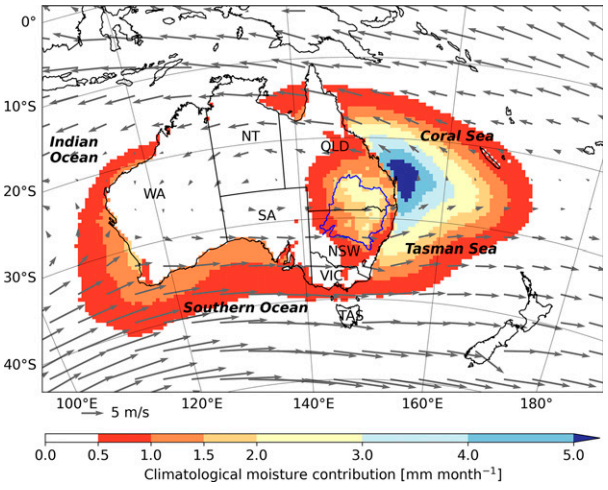

FIG. 1. Climatological June–November moisture contribution to precipitation (mm month^{-1}) in the Northern Murray-Darling Basin (blue polygon) and climatological 850-hPa wind velocity (m s^{-1}). WA = Western Australia; NT = Northern Territory; QLD = Queensland; SA = South Australia; NSW = New South Wales; VIC = Victoria; TAS = Tasmania.

region (Cai et al. 2011b). In contrast, the cold phase of ENSO, La Niña, is associated with enhanced tropical convection concentrated in the Indo-Pacific warm pool north of Australia, which typically results in wetter conditions over eastern Australia (Cai et al. 2012; Risbey et al. 2009). Drier conditions in east Australia are also associated with the positive phase of the IOD, which develops over austral winter and peaks in spring. Positive IOD (+IOD) events are characterized by cold and warm SST anomalies in the eastern and western tropical Indian Ocean, respectively; the converse is true for negative IOD (−IOD) events (Saji et al. 1999). Typically, +IOD events lead to reduced precipitation in southern and eastern parts of Australia (Ashok et al. 2003a; Hauser et al. 2020; Ummenhofer et al. 2010; Meyers et al. 2007). The impacts are generally opposite for −IOD events across the southern parts of Australia (Meyers et al. 2007; Risbey et al. 2009; Verdon and Franks 2005; van Rensch et al. 2015; Gallant et al. 2012), although the degree of impact can vary across studies depending on the analysis period (e.g., Risbey et al. 2009; Ummenhofer et al. 2010). In addition, winter precipitation in east Australia (specifically, parts of central New South Wales and southern Queensland; Fig. 1) can increase during the positive phase of the SAM (+SAM), when the Southern Hemisphere midlatitude storm track migrates southward, and easterly winds from the Tasman Sea are enhanced (Hendon et al. 2007; Meneghini et al. 2007; Cowan et al. 2013). Conversely, eastern Australia is associated with decreased winter precipitation during negative SAM (−SAM) when the storm tracks migrate northward with enhanced atmospheric flow from inland.

Climate modes explain about 20%–40% of east Australian precipitation variability (Risbey et al. 2009). The difficulty in fully characterizing, and thus predicting, east Australia's highly variable precipitation lies in the complex suite of drivers that impact precipitation in different areas on different time and space scales. East Australian precipitation is related to synoptic-scale weather systems including blocking (Risbey et al. 2009; Cowan et al. 2013), meridional troughs (Gallant et al. 2012), cyclones, fronts, and thunderstorms (Pepler et al. 2021), which can be modulated by large-scale climate modes and, on smaller scales, by land–atmosphere interactions (Hirsch et al. 2014; Holgate et al. 2020a). The limited statistical explanation of precipitation variability demonstrates this inherent complexity.

While climate models are now able to simulate modes of climate variability and their teleconnection to Australian precipitation with some degree of fidelity, many features still need significant improvement. Deficiencies are evident in simulating atmospheric blocking (Maher and Sherwood 2016; Ummenhofer et al. 2013; Pook et al. 2010), IOD amplitude and skewness (McKenna et al. 2020; Weller and Cai 2013), ENSO seasonality (McKenna et al. 2020; Taschetto et al. 2014) and associated precipitation bias (Lim et al. 2016), and the interactions between climate modes (Cai et al. 2011b; McKenna et al. 2020; Kajtar et al. 2016)—some of which can be linked to insufficient model resolution and parameterization of atmospheric convection (Guilyardi et al. 2020; Bador et al. 2020). An improved knowledge of how these modes of variability influence precipitation and its moisture sources would help understand how these model biases affect the simulation of Australian climate.

Some studies have reported significant projected changes to ENSO and IOD variability in the future. In particular, the frequency of the most extreme events is projected to increase (Cai et al. 2014) and some of these changes may already be manifesting themselves (Cai et al. 2009; Freund et al. 2019). In addition, there has been a trend toward a more positive SAM over recent decades (Marshall 2003; Thompson and Solomon 2002) with projections indicating that this trend will continue into the future. Without a slowdown in greenhouse gas emissions, the risk of extreme weather events, such as bushfires, droughts, and intense precipitation, is expected to increase (e.g., Abram et al. 2021; Alexander and Arblaster 2017; Bao et al. 2017; Donat et al. 2016; Kirono et al. 2020; Ukkola et al. 2020; Grose et al. 2020). Given the past and possible future changes to these large-scale drivers, it is of particular importance to understand in detail how they modulate Australian precipitation. This would facilitate model development and help us understand the regional impact of long-term changes in these modes.

This study provides a novel perspective to understand the physical links between large-scale climate modes and precipitation by analyzing how important modes of variability modify the supply of evaporative moisture for precipitation. Anomalous precipitation in a region may result from large-scale processes altering the atmospheric moisture supply (by changing evaporation or atmospheric circulation) and/or local-scale processes controlling the conversion of available moisture into precipitation. Using a Lagrangian moisture-tracking approach, we can isolate these influences and shed light on how climate mode–induced dynamic and thermodynamic anomalies translate into precipitation anomalies.

Unauthenticated | Downloaded 01/24/24 02:40 AM UTC

To develop this new perspective, we analyze changes in atmospheric circulation together with evaporation to understand changes to moisture advection into the east Australian region and analyze how local processes modify precipitation. This process pathway can be summarized as follows:

$$\Delta\text{climate mode} \rightarrow \Delta\text{atmospheric circulation} \rightarrow \Delta\text{moisture advection pathways and}$$
$$\Delta\text{evaporation} \rightarrow \Delta\text{local precipitation-triggering/-enhancing processes} \rightarrow \Delta\text{precipitation}.$$

We focus on the northern Murray-Darling Basin (NMDB; Fig. 1), where the amount and timing of precipitation have major socioeconomic importance. For June–November during 1979–2013 and the key modes of ENSO, IOD, and SAM we examine the following questions: How does the interaction of ENSO with the IOD and SAM modify precipitation and its moisture sources for this region? Are the moisture source anomalies a response to thermodynamic or dynamic processes?

2. Methods

a. Back-trajectory model

Evaporative moisture sources for precipitation falling in the NMDB were identified using a three-dimensional (3D) back-trajectory approach with explicit moisture accounting based on Dirmeyer and Brubaker (1999). Moisture supplying precipitation events >2 mm day^{-1} (per grid cell) between 1979 and 2013 was tracked. For each precipitation event at each grid cell, Lagrangian parcels (representative of moist air parcels) were released at a rate proportional to the precipitation rate. Parcels were released from the center of the grid cell from a random height drawn from probability distribution proportional to the total precipitable water profile in the atmosphere, assuming the vertical distribution of precipitable water indicates where the precipitation forms. Each parcel was advected backward in time through the atmosphere using 3D wind fields. At each 10-min time step, part of the parcel's moisture was removed in proportion to the rate at which surface evaporation contributed to column precipitable water at that point in the parcel's trajectory, assuming evaporation mixes well throughout the column during the time step and that evaporation was the only source of moisture for the parcels. Parcels were back-tracked until all precipitable water at the original grid cell was accounted for, or until the parcel reached the edge of the model domain (Fig. 1) or until the maximum back-track time of 30 days was reached, accounting for >92% of total moisture contributing to the region's precipitation (Holgate et al. 2020b). This process yielded daily two-dimensional (2D) maps of evaporative sources that contributed to precipitation falling within the NMDB (Holgate 2021). The primary climatological moisture source region supplying precipitation in the NMDB spans the Tasman and Coral Seas centered between approximately 20° and 30°S (Fig. 1). Important contributions of moisture are also made by the oceans to the north, south, and southwest of the continent. Terrestrial moisture contributions are also made from the east Australian land surface and from the land within the NMDB itself. This terrestrial moisture originating within the NMDB contributes to precipitation recycling. Specifically, the proportion of precipitation falling within the NMDB supplied by terrestrial moisture originating within the same region is known as the precipitation recycling ratio (RR).

The back-trajectory model was driven by 3-hourly 0.5° 3D atmospheric fields of wind, temperature, precipitable water, and pressure and by 2D fields of precipitation and latent heat flux. The fields were produced by an ERA-Interim-driven WRFv3.6.1 regional simulation. The simulation was spectrally nudged with winds and geopotential height above approximately 500 hPa using ERA-Interim to ensure that synoptic-scale systems remained close to the reanalysis. The WRF simulation performed well against observations of temperature and precipitation (Holgate et al. 2020b) and was deemed suitable for the purposes of this study. Annual and winter precipitation bias was low in east Australia, generally within 5 mm month^{-1} of the observations, and fewer than 1% of cells across Australia showed bias of more than 10 mm month^{-1}. Simulated winter minimum and maximum temperatures tended to be underestimated (~1.5 and ~3 K, respectively). Simulated winter evapotranspiration bias in east Australia was approximately −0.5 mm day^{-1} with respect to estimates taken from version 2 of the Derived Optimal Linear Combination Evapotranspiration (DOLCE) dataset, a hybrid of 11 global evapotranspiration datasets (Hobeichi et al. 2020).

Regional precipitation anomalies driven by changes to the climatological moisture supply may arise due to changes in ocean or land evaporation rates (a large-scale thermodynamic response). Alternatively, those source regions may generate the same amount of evaporation, but the contributing moisture redirected elsewhere by shifts in regional or large-scale atmospheric circulation (a dynamic response); or a region may receive the same amount of atmospheric moisture as usual, but local land and atmospheric conditions are not conducive for that moisture to be precipitated (a local thermodynamic response). To distinguish between these drivers of anomalous precipitation, in addition to the moisture sources we also interrogate anomalies in evaporation, total precipitable water, and 500-hPa vertical wind speed. Data were taken from the WRF simulation to remain consistent with the back-trajectory analysis.

b. Moisture source anomalies

To assess the change to precipitation moisture sources during each climate mode phase, moisture source anomalies were computed from the 1979–2013 monthly climatology. The June to November mean climatological moisture source regions for the NMDB are illustrated in Fig. 1. The winter and spring seasons are the focus of our analysis, as precipitation over these

Unauthenticated | Downloaded 01/24/24 02:40 AM UTC

seasons in east Australia tends to be more strongly impacted by the climate modes (e.g., Risbey et al. 2009).

The significance of the anomaly composites during each climate mode phase was assessed using a spatially explicit Monte Carlo bootstrap technique [similar to Tozer et al. (2018)]. For each grid cell, moisture source anomalies in each June–November month over 1979–2013 were sampled randomly 1000 times with replacement to generate one synthetic population distribution for each month. The monthly distributions (n = 1000) were applied to each climate mode phase combination to ensure all phases were tested to the same reference. The anomaly during composited phase months was considered significant if it was more extreme than the resulting distribution's 5th- or 95th-percentile value, indicating the anomaly was unlikely to be obtained purely by chance with 90% confidence (two-tailed). Only those moisture source anomalies considered significant are presented in this study. Additional assessment of the composite variability is provided via precipitation anomalies that occurred during each month contributing to the composite, along with the proportion of months with above- and below-average precipitation (see the online supplemental material).

c. *Classification of climate mode phases*

ENSO months were classed as positive or negative when five or more 3-month (overlapping) averages of Niño-3.4 exceeded ±0.5° based on the classification and ONI time series from NOAA (https://origin.cpc.ncep.noaa.gov/products/analysis_monitoring/ensostuff/ONI_v5.php). IOD months were classed as positive or negative when they exceeded ±0.4° using the Dipole Mode Index (DMI) time series from NOAA (https://psl.noaa.gov/gcos_wgsp/Timeseries/DMI/). SAM months were classed as positive or negative when index values exceeded one standard deviation above or below the 1971–2000 mean, as defined by Marshall (2003), available at https://legacy.bas.ac.uk/met/gjma/sam.html. The monthly evolution of ENSO and its co-occurrence with IOD and SAM during the study period is illustrated in Fig. 2.

3. Results

First, we note that there is in general a relationship between the modes of variability and NMDB precipitation (Fig. 2). There is a negative correlation between mean June–November ENSO and NMDB precipitation (r = −0. 62, $p < 0.001$), in which El Niño corresponds with reduced precipitation while La Niña with increased precipitation. There is also a positive correlation between mean June–November ENSO and IOD (r = 0.47, $p < 0.005$), reflecting the fact that El Niño and La Niña often co-occur with positive and negative IOD events, respectively (Ashok et al. 2003b). However, an asymmetry is noticeable in which the co-occurrence between El Niño and +IOD is more frequent than that of La Niña and −IOD (e.g., Cai et al. 2012; Fig. 2). On the other hand, the correlation between mean June–November ENSO and the SAM index is not significant (r = −0.08, p = 0.65; although spring correlation is stronger: r = −0.3, p = 0.06), with a weak tendency for El Niño to coincide with −SAM and La Niña with +SAM. Given these co-occurrences, an interplay between ENSO and the IOD, and between ENSO and the SAM, is expected, and is examined below. Below we examine moisture sources during standalone El Niño and La Niña events, when the IOD is neutral. This is followed by an examination of standalone IOD events, when ENSO is neutral; we then examine the modulation of ENSO moisture sources by the IOD. A similar analysis is performed for ENSO and SAM.

We examine anomalies in moisture sources (Figs. 3a and 4a) that are computed as deviations from the corresponding monthly NMDB climatological moisture source. Absolute values of moisture contribution are provided in Figs. S1 and S2 in the online supplemental material. Typically, when there is more precipitation than normal there is more moisture supplying those precipitation events. Thus positive anomalies indicate regions where more moisture than normal was sourced, ultimately contributing to precipitation over the NMDB, during the given phase combination. Conversely, negative anomalies indicate regions where less moisture than normal was sourced that contributed to NMDB precipitation. Likewise, deviations from the climatological surface evaporation, total precipitable water, and 500-hPa vertical wind speed are provided in Figs. 3 and 4b–d, respectively, to complement the moisture source analysis.

a. *ENSO and IOD*

1) Standalone El Niño and La Niña (when IOD is neutral)

We begin by examining moisture sources during standalone ENSO events, when IOD conditions are neutral. During standalone La Niña events [Fig. 3a(ii)] circulation shifts in the western Pacific direct additional moisture from the ocean directly east of Australia, centered between 20° and 30°S (Fig. 1), toward the NMDB. This favorable circulation conspires with greater amounts of atmospheric moisture [+15% in the NMDB; Fig. 3c(ii)] and greater vertical uplift [+20%; Fig. 3d(ii)] to result in an enhanced supply of moisture to and subsequent precipitation within the NMDB during standalone La Niña events.

During standalone El Niño events [Fig. 3a(vi)] precipitation, and therefore the moisture supplying that precipitation, were below average. In other words, less moisture was required to be back-tracked to account for all precipitation during this phase. Precipitation and moisture contribution anomalies are not associated with statistically significant changes in total precipitable water above the NMDB itself [Fig. 3c(vi)]. In contrast to standalone La Niña, suppressed vertical uplift over the region [−19% over the NMDB; Fig. 3d(vi)] leads to below-average precipitation (in 82% of El Niño–neutral IOD months; Fig. S3h).

2) Standalone IOD (when ENSO is neutral)

We next consider moisture sources during standalone IOD events when ENSO conditions are neutral. Negative IOD months are associated with weakened climatological easterlies (Fig. 1), resulting in anomalous westerly flow over northern

Unauthenticated | Downloaded 01/24/24 02:40 AM UTC

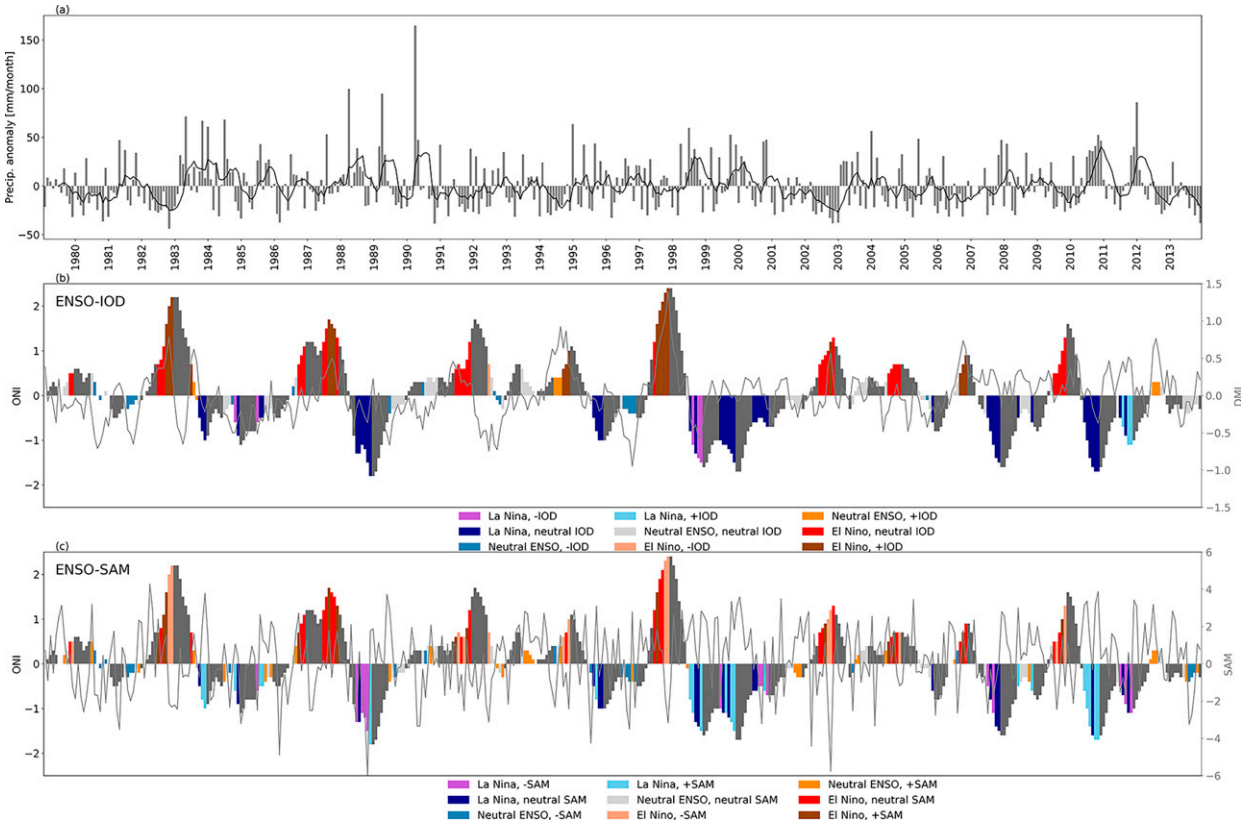

FIG. 2. Time series of monthly (a) NMDB precipitation anomalies (gray bars) with a 6-month running mean (black line), (b) ONI (left axis) bars shaded based on June–November phase combination with DMI (gray line, right axis), and (c) ONI (left axis) bars shaded based on June–November phase combination with SAM (gray line, right axis). In (b) and (c), months outside of June–November are shaded in dark gray.

Australia and the NMDB [Fig. 3a(iii)], which weakened advection of moisture from parts of the Tasman–Coral Sea source region. Little change to local evaporation [Fig. 3b(iii)] or total precipitable water [Fig. 3c(iii)] is evident during standalone −IOD events, although regional uplift is enhanced compared to normal [Fig. 3d(iii)]. Overall, these changes result in a modest positive precipitation anomaly averaged over all standalone −IOD months [+4.5 mm month^{-1}; Fig. 3a(iii)], although precipitation during these periods tends to be somewhat variable, with 62% of months experiencing above-average precipitation (Fig. S3d).

Standalone +IOD events are associated with anomalous broad-scale easterly flow across the continent [Fig. 3a(v)], reduced precipitable water [−14% in the NMDB; Fig. 3c(v)], and enhanced subsidence [−22% in the NMDB; Fig. 3d(v)] that together result in reduced precipitation [Fig. 3a(v); see also Fig. S3f]. The moisture supplied to precipitation events in this phase was lower than normal from the waters around the western, southern, and eastern parts of Australia. The reduced marine moisture supply coincides with decreased marine evaporation off the western, southeastern, and southern coasts of the continent [Fig. 3b(v)]. Although a region of strong positive evaporation anomaly is evident in the Coral Sea [~10°–20°S; Fig. 3b(v)], this source of moisture does not directly increase the precipitable water available to the NMDB.

3) MODULATION OF ENSO BY IOD

When La Niña and −IOD co-occur, moisture supply from the Tasman/Coral Sea source region is strongly enhanced [Fig. 3a(i)], along with widespread increases in total precipitable water [+15% in the NMDB; Fig. 3c(i)]. Together with enhanced large-scale vertical uplift [+34% in the NMDB; Fig. 3d(i)], the co-occurrence of La Niña and −IOD results in above-average precipitation in the NMDB [+15.9 mm month^{-1}; Fig. 3a(i)]. Enhanced terrestrial evaporation in and to the north of the NMDB is also evident, elevating precipitation recycling in this phase [Fig. 3b(i)]. Interestingly, very strong positive anomalies in marine evaporation are evident in the tropical Indian Ocean off the northwest of Australia during La Niña and −IOD [Fig. 3b(i)], but do not directly contribute to the increased supply of moisture for precipitation in the NMDB [Fig. 3a(i)].

When El Niño and +IOD co-occur, anticyclonic motion associated with prevailing high pressure to the south of the continent results in a weak increase in moisture advected from the Tasman Sea [Fig. 3a(vii)]. This is more than compensated by negative moisture source anomalies across the

Unauthenticated | Downloaded 01/24/24 02:40 AM UTC

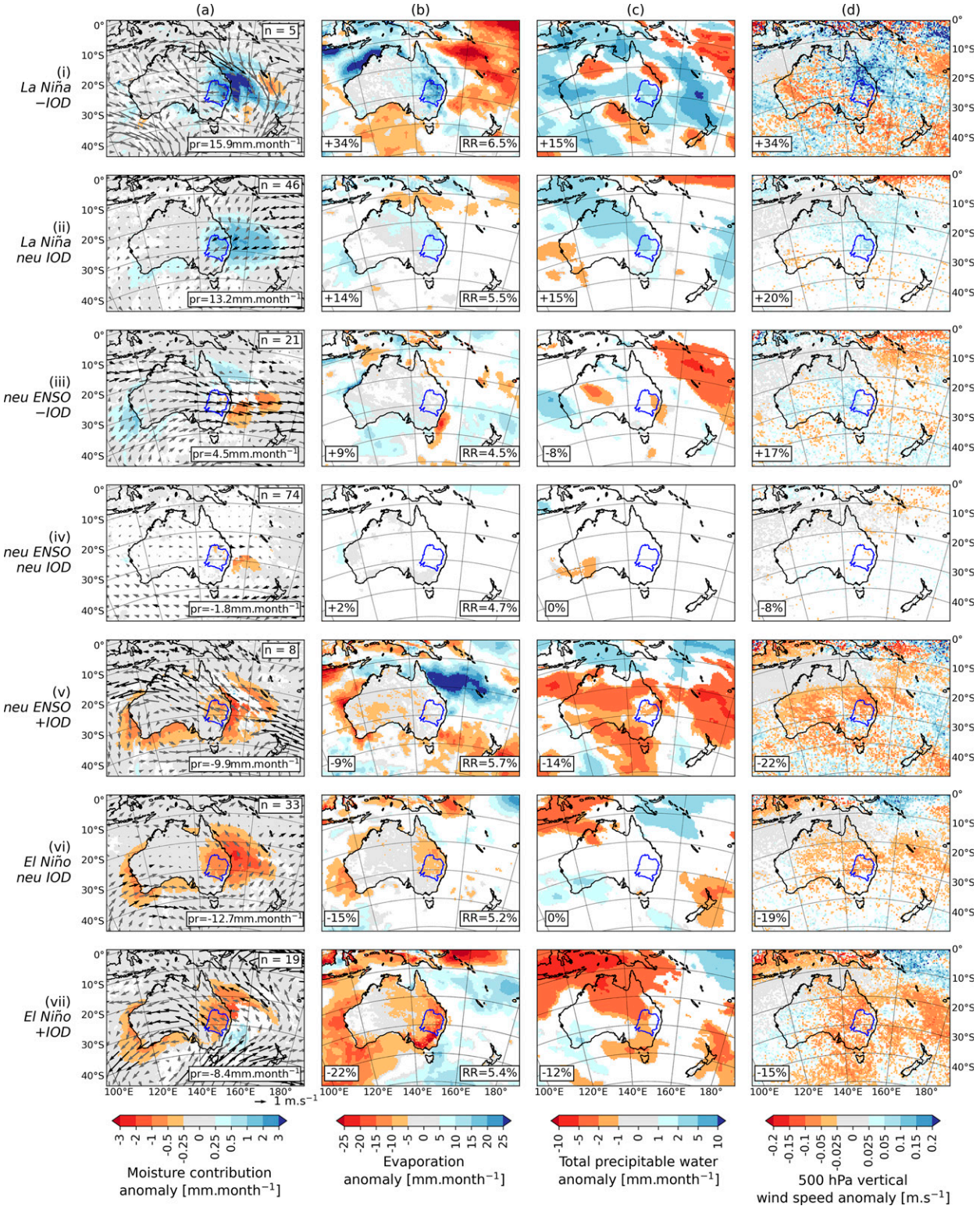

FIG. 3. June–November anomalies during combined phases of ENSO and IOD. (a) NMDB moisture source anomalies (for precipitation events > 2 mm day^{-1}), overlaid by 850-hPa wind anomalies. The number of months (n) making up each composite is given in the top-right corner, with the mean precipitation anomaly in the bottom-right corner. (b)–(d) Anomalies of evaporation, total precipitable water, and 500-hPa maximum vertical wind speed, respectively. The mean anomaly across the NMDB, expressed as a percentage of climatology, is given in the bottom-left corner. The mean precipitation recycling ratio (RR) is given in the bottom-right corner of (b). Anomalies are only shown where they are statistically significant at the 90% confidence level (two-tailed) based on bootstrapping with 1000 samples. Black vectors in (a) denote anomalies that are significant at the 90% confidence level as estimated by a two-tailed t test.

Unauthenticated | Downloaded 01/24/24 02:40 AM UTC

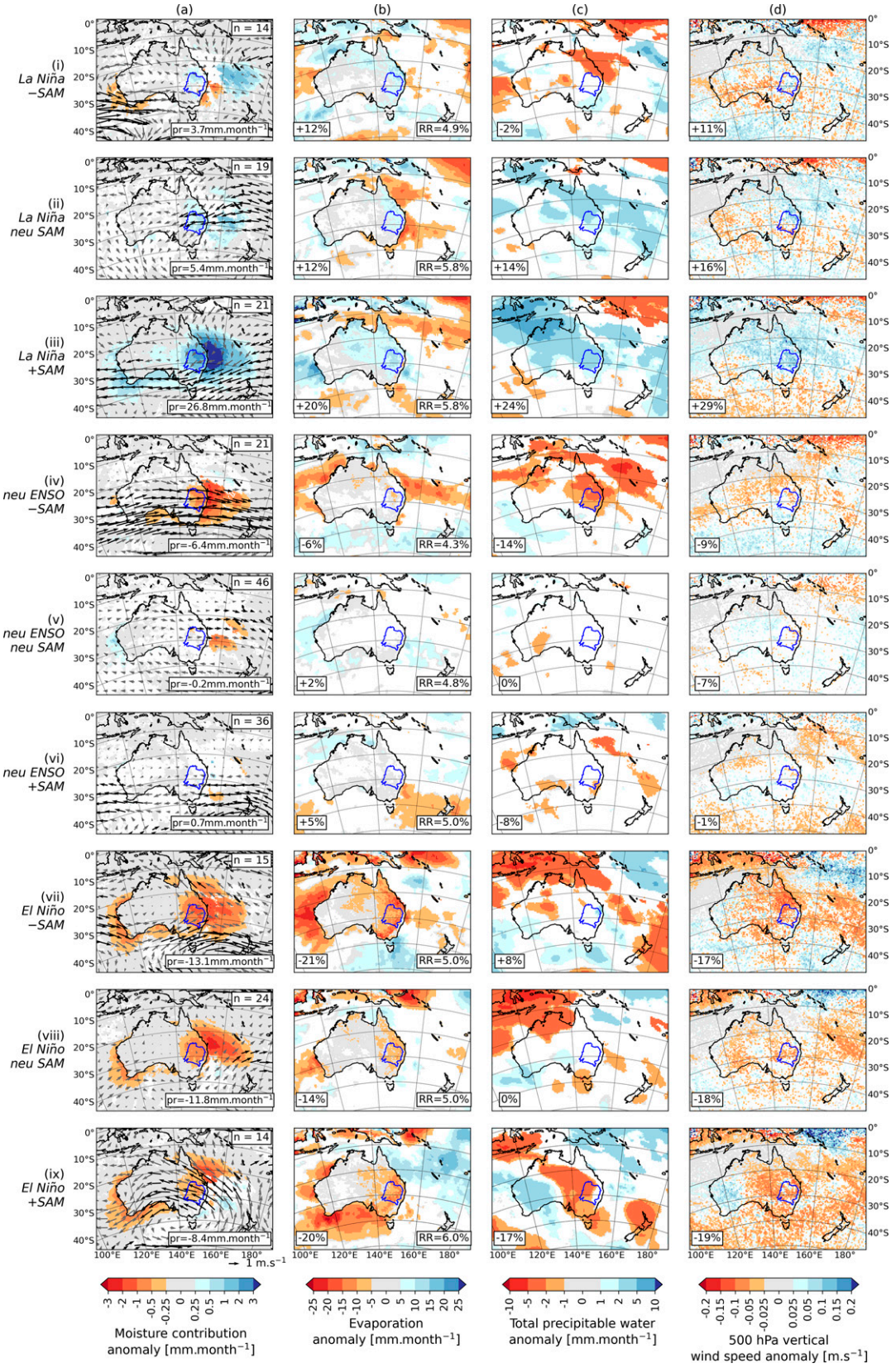

FIG. 4. As for Fig. 3, but for ENSO and SAM.

Unauthenticated | Downloaded 01/24/24 02:40 AM UTC

southern Coral Sea, to the south and west of Australia also found during standalone El Niño [Fig. 3a(vi)]. The anticyclonic motion south of the continent is consistent with an anomalous high pressure center that forms part of Rossby wave trains associated with +IOD events (McIntosh and Hendon 2018; Cai et al. 2011b), although further work is needed to directly link wave activity with precipitation moisture supply. Terrestrial evaporation is considerably reduced over the NMDB (−22%) and eastern half of Australia [Fig. 3b(vii)], a result that is reflected in the negative anomaly in terrestrial moisture contributed to the NMDB from this area [Fig. 3a(vii)]. Together these processes result in reduced precipitable water over the NMDB [−12%; Fig. 3c(vii)] and, combined with enhanced regional subsidence [−15% over the NMDB; Fig. 3d(vii)], lead to below-average precipitation during co-occurring El Niño and +IOD months.

b. *ENSO and SAM*

1) Standalone El Niño and La Niña (when SAM is neutral)

We next consider the impact of standalone La Niña and El Niño to moisture supply when SAM is neutral (without consideration of the IOD). During standalone La Niña, a smaller increase in moisture supply is evident [Fig. 4a(ii)] compared to standalone La Niña months when IOD was neutral [Fig. 3a(ii)], noting the smaller sample size in the latter case. The increased supply of moisture is not due to increased evaporation in the primary marine source region [when it in fact decreased; Fig. 4b(ii)] but rather due to elevated precipitable water in the NMDB (+14%) and wider region [Fig. 4c(ii)]. Together with a net increase in vertical uplift [+16%; Fig. 4d(ii)] in the NMDB, standalone La Niña months experience precipitation that is above average [Fig. 4a(ii)].

During standalone El Niño [Fig. 4a(viii)], negative moisture source anomalies are similar in spatial extent and magnitude to those evident during standalone El Niño when IOD was neutral [Fig. 3a(vi)]. As was the case for standalone El Niño when IOD was neutral, the below-average precipitation during standalone El Niño seen here appears to be driven by suppressed vertical uplift [−18%; Fig. 4d(viii)] and not due to significant changes in the amount of locally available precipitable water [Fig. 4c(viii)].

2) Standalone SAM (when ENSO is neutral)

During standalone −SAM months, the climatological westerly winds across southern Australia (Fig. S2d) are strengthened in association with the equatorward shift of the midlatitude westerlies [Fig. 4a(iv)]. This strengthening of the westerlies clearly inhibits easterly flow of marine moisture into the NMDB and increases the flow of drier air from the continental interior. This is compounded by a reduction in evaporation to the east of Australia between ~20° and 30°S. This phase is also associated with reductions in precipitable water in the NMDB (−14%) and surroundings [Fig. 4c(iv)]. There is also a moderate reduction in vertical uplift associated with a large-scale band of anomalous subsidence across the Australian subtropics [−9%; Fig. 4d(iv)]. Therefore, the below-average precipitation evident during standalone −SAM appears to be a result of a reduction in both the local atmospheric moisture and the uplift of that moisture.

Standalone +SAM appears to have very little impact on the NMDB's July–November moisture sources or precipitation [Fig. 4a(vi)]. This is because precipitation during standalone +SAM tends to be quite variable, with 53% (47%) of months experiencing above (below) average precipitation (Fig. S4f), overall leading to a minor mean change [Fig. 4a(vi)].

3) Modulation of ENSO by SAM

When La Niña and −SAM co-occur [Fig. 4a(i)], the enhanced westerly flow associated with standalone −SAM [Fig. 4a(iv)] suppresses the anomalous easterly flow of moisture from the Coral Sea into the NMDB otherwise seen during standalone La Niña [Fig. 4a(ii)]. Overall, this acts to reduce positive moisture and precipitation anomalies [Fig. 4a(i)] compared to standalone La Niña [Fig. 4a(ii)]. The impact of standalone La Niña is dampened when −SAM co-occurs with La Niña, as elevated levels of locally available atmospheric moisture are reduced from +14% [Fig. 4c(ii)] to −2% [Fig. 4c(i)], and the positive anomaly in vertical uplift is reduced from +16% [Fig. 4d(ii)] to +11% [Fig. 4d(i)]. These changes result in a smaller overall impact to moisture supply and precipitation [Fig. 4a(i)] when La Niña and −SAM co-occur compared to standalone La Niña [Fig. 4a(ii)], and compared to when −SAM and El Niño co-occur [Fig. 4a(vii)].

The co-occurrence of La Niña and +SAM has the largest effect on the NMDB of all the mode combinations, intensifying positive moisture source anomalies to result in above-average precipitation [Fig. 4a(iii)]. Moisture supply is strongly enhanced in the adjacent ocean between 20° and 35°S associated with strengthened northeasterly flow that brings moist marine air toward the NMDB [Fig. 4a(iii)], despite relatively small collocated increases in ocean evaporation [Fig. 4b(iii)]. More moderate enhanced moisture supply is also evident from the southwest coast of Australia, which is associated with upper-level flows circulating Southern Ocean marine moisture back toward the NMDB (not shown). In this combined phase, total precipitable water is considerably increased in the NMDB (+24%) and wider region [Fig. 4c(iii)]. Vertical uplift increases considerably [+29% over the NMDB; Fig. 4d(iii)], associated with a large-scale band of enhanced uplift over the Australian subtropics. The enhancement of uplift over the subtropics, and subsidence over the midlatitudes, that are evident during standalone +SAM months [Fig. 4d(vi)] intensify when La Niña and +SAM co-occur [Fig. 4d(iii)]. Together, these processes conspire to produce above-average precipitation in 86% of La Niña and +SAM co-occurring months (Fig. S4c).

Note that +SAM does not have an equal and opposite impact when co-occurring with El Niño. During combined El Niño and +SAM months, the low moisture supply from the waters off the southwest coast of Australia is exacerbated [Fig. 4a(ix)], but the negative anomaly in the Tasman Sea source region is slightly lessened, compared to standalone El Niño [Fig. 4a(viii)]. There is a reduction in the amount of atmospheric moisture available for precipitation in the

Unauthenticated | Downloaded 01/24/24 02:40 AM UTC

NMDB, evident from reductions in both local (−20%) and regional terrestrial evaporation [Fig. 4b(ix)] and local (−17%) and regional precipitable water [Fig. 4c(ix)]. The reduction in available moisture and the suppressed vertical uplift in the region [−19% over the NMDB; Fig. 4d(ix)] result in below-average precipitation during this phase [Fig. 4a(ix)].

When El Niño and −SAM co-occur, the geographic area of low moisture supply from the waters to the west, south, and east of the continent is broadened [Fig. 4a(vii)] compared to standalone El Niño [Fig. 4a(viii)]. Despite this, and also despite a marked reduction in the amount of moisture contributed to the atmosphere by local (−21%) and proximate terrestrial evaporation [Fig. 4b(vii)], only a relatively small change in available precipitable water within the NMDB is evident [+8%; Fig. 4c(vii)]. Instead, the below-average precipitation appears to be driven by widespread subsidence [−17% over the NMDB; Fig. 4d(vii)].

4. Discussion

a. ENSO

Our analysis shows that during standalone La Niña there is considerably more atmospheric moisture available in the region and the resultant circulation anomalies are favorable to transporting more of that moisture toward east Australia. While the anomalous moisture sources for standalone El Niño tend to be opposite to those of standalone La Niña, there are asymmetries in terms of magnitude and the contributing processes (Fig. 3). For instance, during standalone La Niña, the dynamic change to moisture transport is associated with increases in precipitable water and ascending motion that facilitate local thermodynamic precipitation-generating processes, which together result in above-average winter–spring precipitation. During standalone El Niño, on the other hand, below-average precipitation is associated with strongly enhanced subsidence. Such asymmetry could arise from nonlinearity in ENSO phases in the tropical Pacific, whereby El Niño SST anomalies tend to be larger than La Niña ones, and El Niño SST anomalies tend to be located more eastward than La Niña events (e.g., Santoso et al. 2017), which are more consistently confined to the central Pacific (Chung and Power 2017; Frauen et al. 2014). The latter might explain why the anomalous circulation over east Australia is more pronounced during standalone La Niña than El Niño [Figs. 3a(ii),(vi)], associated with the more apparent Pacific–South American (PSA) pattern, a mechanism for ENSO-teleconnection to the extratropics, during La Niña rather than El Niño (Cai et al. 2012).

Our results are consistent with the findings of previous work that showed a connection between strengthening of northerly flow from the tropics and wetter conditions during standalone La Niña and southerly flow and drier conditions during standalone El Niño (van Rensch et al. 2019; Cowan et al. 2013). Our results are also consistent with previous research focusing specifically on the 2010/11 La Niña event. Ummenhofer et al. (2015) concluded that the enhanced east Australian precipitation during the event was a result of enhanced ascending motion over eastern and northeastern Australia and over the ocean to the north of the continent, combined with stronger onshore moisture transport and convergence. We show, specifically, that La Niña events typically act to increase the easterly and northeasterly advection of marine moisture from the Coral and Tasman Seas into east Australia, and combined with enhanced vertical uplift, leads to anomalously high precipitation.

Our results are also consistent with previous studies using back-trajectory analysis to identify moisture sources for precipitation from cutoff low systems in southeast Australia (McIntosh et al. 2012; Brown et al. 2009; McIntosh et al. 2007). The authors showed that during cutoff low events moisture was sourced from the ocean to the northeast of Australia (McIntosh et al. 2012, 2007) including during the 1997 El Niño (Brown et al. 2009). Extending this work with 35 years of data, our results identify the ocean to the northeast and east of Australia as a consistent source of moisture for east Australian precipitation during ENSO, IOD, and SAM phases.

b. ENSO and IOD

Our analysis shows that processes contributing to NMDB precipitation moisture sources intensify when the IOD co-occurs with ENSO, compared to standalone ENSO. The IOD influence on ENSO is not symmetric, however, and is likely affected by differences in strength (Cai et al. 2012; Santoso et al. 2017) and frequency (Fig. 3) of +IOD and −IOD. Although co-occurring phases of both La Niña/−IOD and El Niño/+IOD were associated with an intensification of the ENSO-related anomalies in precipitable water and atmospheric uplift on a broad scale, the impact on precipitation and moisture sources of the NMDB is more nuanced. Within the NMDB, La Niña/−IOD maintained (but did not increase) the mean level of local atmospheric moisture otherwise available during standalone La Niña, but enhanced vertical uplift, leading to a slightly larger precipitation anomaly compared to standalone La Niña. On the other hand, El Niño/+IOD reduced the amount of atmospheric moisture in the NMDB during El Niño but had only a small effect on local subsidence, leading to a slightly smaller precipitation anomaly compared to standalone El Niño. These results refine the broad-scale Indian–Pacific Ocean moisture transport processes for co-occurring ENSO/IOD phases inferred by Rathore et al. (2020).

While we have shown that anomalies are intensified when ENSO and IOD co-occur, the relative role played by each mode is not easily distinguished when they are both active. For instance, months of El Niño and +IOD co-occurrence tend to occur after El Niño has been present for some months (Fig. 2), so there could also be some impact from antecedent El Niño conditions not considered in our analysis. A process-based investigation of the relative roles during periods when both modes are active, and between diverse ENSO events, represents an avenue for future research.

c. ENSO and SAM

Our results show that winter–spring NMDB precipitation and moisture sources during −SAM months are impacted by strengthened westerlies and associated changes to the

Unauthenticated | Downloaded 01/24/24 02:40 AM UTC

transport of moisture into the NMDB. This modification of atmospheric circulation and moisture transport dampens the impact of standalone La Niña by strongly reducing the high levels of atmospheric moisture and uplift otherwise seen during standalone La Niña.

Like −SAM, during +SAM months our results indicate that NMDB precipitation and moisture sources are affected by modified circulation. In the case of +SAM, precipitation is affected via anomalous easterly flow modulating moisture transport into the region, as suggested by previous studies (Cowan et al. 2013; Gillett et al. 2006; Sen Gupta and England 2006; Hendon et al. 2007; Pui et al. 2012). Importantly, our results reveal that the impact of easterly advection during +SAM differs depending on the background state of ENSO. The impact of standalone La Niña is exacerbated during La Niña/+SAM months by a strengthening of anomalous easterly advection of moist marine air into the region. On the other hand, the impact to easterly flow tends to dampen the dry anomaly evident during standalone El Niño. This is despite a greater reduction in local atmospheric moisture during co-occurring El Niño/+SAM compared to standalone El Niño, suggesting that precipitation impacts are more strongly driven by the El Niño–related subsidence in this combined phase. Moreover, the fact that the effect of +SAM depends on the state of ENSO adds nuance to previous work showing increased east Australian precipitation during +SAM results from increased moisture transport from the tropical Indian and western Pacific Oceans (Nieto et al. 2014; Cowan et al. 2013).

The capacity of the combined phase of La Niña and +SAM to strongly impact east Australian precipitation has also been shown previously. Analyzing an instance of interaction between La Niña and a highly positive SAM, Hendon et al. (2013) demonstrated that +SAM contributed up to 40% of the extreme east Australian precipitation during the record wet spring of 2010. During 2010, La Niña acted to weaken the subtropical jet and the resulting adiabatic warming in the mid-latitudes promoted the development of a highly positive SAM (Lim and Hendon 2015).

5. Conclusions

This study sought to offer a new perspective on the physical connection between important modes of climate variability and east Australian precipitation, by investigating the changes to moisture sources during individual and combined phases of ENSO, IOD, and SAM. More broadly, the framework presented in this study offers a template for examining regional precipitation processes in other parts of the world similarly subject to large-scale modes of climate variability.

Our results are summarized as follows:

- The response of east Australian precipitation and its moisture sources to ENSO consists of a combined dynamic–thermodynamic response to La Niña, and a local thermodynamic response to broad-scale El Niño dynamic anomalies. During La Niña, dynamic changes to moisture transport combine with enhanced ascending motion to facilitate local thermodynamic precipitation-generating processes, leading to wetter conditions. During El Niño, the latter process is responsible for dry conditions, as greater regional subsidence suppresses local precipitation-generating processes over east Australia.
- When ENSO and IOD co-occur the sign of the ENSO-related precipitation and moisture source anomalies was maintained, considering the prevalent co-occurrence between +IOD and El Niño and between −IOD and La Niña. In addition to increased subsidence evident during standalone El Niño events, months when El Niño and +IOD combined were associated with reduced moisture transport into the region and below-average precipitation. On the other hand, compared to standalone La Niña events, months when La Niña and −IOD co-occurred were associated with greater vertical uplift, moisture availability and precipitation.
- When ENSO and SAM co-occur, changes to atmospheric circulation, through the strengthening or weakening of the climatological westerlies, impacted the transport of moisture for precipitation. Compared to standalone ENSO events, we found greater impacts on east Australian precipitation and its moisture sources when La Niña and +SAM co-occurred, and dampened impacts when El Niño and +SAM co-occurred, with −SAM having the reverse effect.

Building on the framework presented in this study, future work may consider the impact of other processes important for east Australian precipitation such as the position and intensity of the subtropical ridge and blocking (e.g., Cai et al. 2011a; Cowan et al. 2013; Risbey et al. 2009), the Madden–Julian oscillation (e.g., Lim et al. 2021), northwest cloud bands (e.g., Black et al. 2021; Reid et al. 2019), and the differences between eastern and central Pacific El Niño events (Freund et al. 2021). Future studies may also investigate whether the strengthened subsidence during El Niño is the direct cause of reduced precipitation frequency, or rather the signature of fewer precipitation-generating systems, including whether there are fewer events or fewer precipitation-bearing events. The work could also be extended to examine how different storm types impact precipitation of varying intensity and associated moisture sources, and how the impact is modified by the interaction of large-scale climate modes and local-scale terrestrial processes.

Acknowledgments. This work was possible thanks to an Australian National University AGRT Scholarship (C.M.H.) and support from the ARC Centre of Excellence for Climate System Science (CE110001028). J.P.E., A.S.T, A.S.G., and A.S. were supported via the ARC Centre of Excellence for Climate Extremes (CE170100023). A.S. is supported by the Centre for Southern Hemisphere Oceans Research (CSHOR), a joint research center between QNLM and CSIRO. J.P.E., A.S.T. and A.S. acknowledge support from the Australian Government's National Environmental Science Program. The authors thank the National Computing Infrastructure and its staff for the computational support. The authors thank A. Marshall, J. Risbey, and one anonymous reviewer for their help in improving the manuscript.

Data availability statement. CORDEX-Australasia climate simulations used in this study are publicly available (https://

Unauthenticated | Downloaded 01/24/24 02:40 AM UTC

climatedata.environment.nsw.gov.au/). The evaporative source regions derived from the back-trajectory analysis are publicly available (https://doi.org/10.25914/616ea51ea5afd).

REFERENCES

Abram, N. J., and Coauthors, 2021: Connections of climate change and variability to large and extreme forest fires in southeast Australia. *Commun. Earth Environ.*, **2**, 8, https://doi.org/10.1038/s43247-020-00065-8.

Alexander, L. V., and J. M. Arblaster, 2017: Historical and projected trends in temperature and precipitation extremes in Australia in observations and CMIP5. *Wea. Climate Extremes*, **15**, 34–56, https://doi.org/10.1016/j.wace.2017.02.001.

Arblaster, J. M., and L. V. Alexander, 2012: The impact of the El Niño–Southern Oscillation on maximum temperature extremes. *Geophys. Res. Lett.*, **39**, L20702, https://doi.org/10.1029/2012GL053409.

Ashok, K., Z. Guan, and T. Yamagata, 2003a: Influence of the Indian Ocean Dipole on the Australian winter rainfall. *Geophys. Res. Lett.*, **30**, https://doi.org/10.1029/2003GL017926.

——, ——, and ——, 2003b: A look at the relationship between the ENSO and the Indian Ocean Dipole. *J. Meteor. Soc. Japan*, **81**, 41–56, https://doi.org/10.2151/jmsj.81.41.

Bador, M., and Coauthors, 2020: Impact of higher spatial atmospheric resolution on precipitation extremes over land in global climate models. *J. Geophys. Res. Atmos.*, **125**, e2019JD032184, https://doi.org/10.1029/2019JD032184.

Bao, J., S. C. Sherwood, L. V. Alexander, and J. P. Evans, 2017: Future increases in extreme precipitation exceed observed scaling rates. *Nat. Climate Change*, **7**, 128–132, https://doi.org/10.1038/nclimate3201.

Black, A. S., and Coauthors, 2021: Australian northwest cloudbands and their relationship to atmospheric rivers and precipitation. *Mon. Wea. Rev.*, **149**, 1125–1139, https://doi.org/10.1175/MWR-D-20-0308.1.

Brown, J. N., P. C. McIntosh, M. J. Pook, and J. S. Risbey, 2009: An investigation of the links between ENSO flavors and rainfall processes in southeastern Australia. *Mon. Wea. Rev.*, **137**, 3786–3795, https://doi.org/10.1175/2009MWR3066.1.

Cai, W., A. Sullivan, and T. Cowan, 2009: Climate change contributes to more frequent consecutive positive Indian Ocean Dipole events. *Geophys. Res. Lett.*, **36**, L23704, https://doi.org/10.1029/2009GL040163.

——, P. van Rensch, and T. Cowan, 2011a: Influence of global-scale variability on the subtropical ridge over southeast Australia. *J. Climate*, **24**, 6035–6053, https://doi.org/10.1175/2011JCLI4149.1.

——, ——, ——, and H. H. Hendon, 2011b: Teleconnection pathways of ENSO and the IOD and the mechanisms for impacts on Australian rainfall. *J. Climate*, **24**, 3910–3923, https://doi.org/10.1175/2011JCLI4129.1.

——, ——, ——, and ——, 2012: An asymmetry in the IOD and ENSO teleconnection pathway and its impact on Australian climate. *J. Climate*, **25**, 6318–6329, https://doi.org/10.1175/JCLI-D-11-00501.1.

——, and Coauthors, 2014: Increasing frequency of extreme El Niño events due to greenhouse warming. *Nat. Climate Change*, **4**, 111–116, https://doi.org/10.1038/nclimate2100.

Chiew, F. H. S., T. C. Piechota, J. A. Dracup, and T. A. McMahon, 1998: El Niño/Southern Oscillation and Australian rainfall, streamflow and drought: Links and potential for forecasting. *J. Hydrol.*, **204**, 138–149, https://doi.org/10.1016/S0022-1694(97)00121-2.

Chung, C. T. Y., and S. B. Power, 2017: The non-linear impact of El Niño, La Niña and the Southern Oscillation on seasonal and regional Australian precipitation. *J. South. Hemisphere Earth Syst. Sci.*, **67**, 25–45, https://doi.org/10.22499/3.6701.003.

Cowan, T., P. van Rensch, A. Purich, and W. Cai, 2013: The association of tropical and extratropical climate modes to atmospheric blocking across southeastern Australia. *J. Climate*, **26**, 7555–7569, https://doi.org/10.1175/JCLI-D-12-00781.1.

Dirmeyer, P. A., and K. L. Brubaker, 1999: Contrasting evaporative moisture sources during the drought of 1988 and the flood of 1993. *J. Geophys. Res.*, **104**, 19 383–19 397, https://doi.org/10.1029/1999JD900222.

Donat, M. G., A. L. Lowry, L. V. Alexander, P. A. O'Gorman, and N. Maher, 2016: More extreme precipitation in the world's dry and wet regions. *Nat. Climate Change*, **6**, 508–513, https://doi.org/10.1038/nclimate2941.

Evans, J. P., and I. Boyer-Souchet, 2012: Local sea surface temperatures add to extreme precipitation in northeast Australia during La Niña. *Res. Lett.*, **39**, L10803, https://doi.org/10.1029/2012GL052014.

Frauen, C., D. Dommenget, N. Tyrrell, M. Rezny, and S. Wales, 2014: Analysis of the nonlinearity of El Niño–Southern Oscillation teleconnections. *J. Climate*, **27**, 6225–6244, https://doi.org/10.1175/JCLI-D-13-00757.1.

Freund, M. B., B. J. Henley, D. J. Karoly, H. V. McGregor, N. J. Abram, and D. Dommenget, 2019: Higher frequency of Central Pacific El Niño events in recent decades relative to past centuries. *Nat. Geosci.*, **12**, 450–455, https://doi.org/10.1038/s41561-019-0353-3.

——, A. G. Marshall, M. C. Wheeler, and J. N. Brown, 2021: Central Pacific El Niño as a precursor to summer drought-breaking rainfall over southeastern Australia. *Geophys. Res. Lett.*, **48**, e2020GL091131, https://doi.org/10.1029/2020GL091131.

Gallant, A. J. E., A. S. Kiem, D. C. Verdon-Kidd, R. C. Stone, and D. J. Karoly, 2012: Understanding hydroclimate processes in the Murray-Darling Basin for natural resources management. *Hydrol. Earth Syst. Sci.*, **16**, 2049–2068, https://doi.org/10.5194/hess-16-2049-2012.

Gillett, N. P., T. D. Kell, and P. D. Jones, 2006: Regional climate impacts of the Southern Annular Mode. *Geophys. Res. Lett.*, **33**, L23704, https://doi.org/10.1029/2006GL027721.

Glantz, M. H., 2001: *Currents of Change: Impacts of El Niño and La Niña on Climate and Society*. 2nd ed. Cambridge University Press, 268 pp.

Grose, M. R., and Coauthors, 2020: Insights from CMIP6 for Australia's future climate. *Earth's Future*, **8**, e2019EF001469, https://doi.org/10.1029/2019EF001469.

Guilyardi, E., A. Capotondi, M. Lengaigne, S. Thual, and A. T. Wittenberg, 2020: ENSO modelling: History, progress and challenges. *El Niño Southern Oscillation in a Changing Climate*, W. McPhaden, M. J. Santoso, and A. Cai, Eds., Amer. Geophys. Union, 199–226.

Hauser, S., C. M. Grams, M. J. Reeder, S. McGregor, A. H. Fink, and J. F. Quinting, 2020: A weather system perspective on winter–spring rainfall variability in southeastern Australia during El Niño. *Quart. J. Roy. Meteor. Soc.*, **146**, 2614–2633, https://doi.org/10.1002/qj.3808.

Hendon, H. H., D. W. J. Thompson, and M. C. Wheeler, 2007: Australian rainfall and surface temperature variations associated with the Southern Hemisphere annular mode. *J. Climate*, **20**, 2452–2467, https://doi.org/10.1175/JCLI4134.1.

Unauthenticated | Downloaded 01/24/24 02:40 AM UTC

——, E.-P. Lim, J. M. Arblaster, and D. L. T. Anderson, 2013: Causes and predictability of the record wet east Australian spring 2010. *Climate Dyn.*, **42**, 1155–1174, https://doi.org/10.1007/s00382-013-1700-5.

Hirsch, A. L., A. J. Pitman, S. I. Seneviratne, J. P. Evans, and V. Haverd, 2014: Summertime maximum and minimum temperature coupling asymmetry over Australia determined using WRF. *Geophys. Res. Lett.*, **41**, 1546–1552, https://doi.org/10.1002/2013GL059055.

Hobeichi, S., G. Abramowitz, and J. P. Evans, 2020: Derived Optimal Linear Combination Evapotranspiration—DOLCE v2.0. Research Data Australia, accessed 14 May 2020, https://doi.org/10.25914/5eab8f533aeae.

Holgate, C. M., 2021: Evaporative source regions for Australian precipitation from Lagrangian back-trajectory analysis v1.0. Research Data Australia, accessed 15 October 2020, https://doi.org/10.25914/616ea51ea5afd.

——, A. I. J. M. van Dijk, J. P. Evans, and A. J. Pitman, 2020a: Local and remote drivers of southeast Australian drought. *Geophys. Res. Lett.*, **47**, e2020GL090238, https://doi.org/10.1029/2020GL090238.

——, J. P. Evans, A. I. J. M. van Dijk, J. Pitman, and G. Di Virgilio, 2020b: Australian precipitation recycling and evaporative source regions. *J. Climate*, **33**, 8721–8735, https://doi.org/10.1175/JCLI-D-19-0926.1.

Iizumi, T., J. J. Luo, A. J. Challinor, G. Sakurai, M. Yokozawa, H. Sakuma, M. E. Brown, and T. Yamagata, 2014: Impacts of El Niño Southern Oscillation on the global yields of major crops. *Nat. Commun.*, **5**, 3712, https://doi.org/10.1038/ncomms4712.

Jones, D. A., and B. C. Trewin, 2000: On the relationships between the El Niño–southern oscillation and Australian land surface temperature. *Int. J. Climatol.*, **20**, 697–719, https://doi.org/10.1002/1097-0088(20000615)20:7<697::AID-JOC499>3.0.CO;2-A.

Kajtar, J. B., A. Santoso, M. H. England, and W. Cai, 2016: Tropical climate variability: Interactions across the Pacific, Indian, and Atlantic Oceans. *Climate Dyn.*, **487**, 2173–2190, https://doi.org/10.1007/s00382-016-3199-z.

Kirono, D. G. C., V. Round, C. Heady, F. H. S. Chiew, and S. Osbrough, 2020: Drought projections for Australia: Updated results and analysis of model simulations. *Wea. Climate Extremes*, **30**, 100280, https://doi.org/10.1016/j.wace.2020.100280.

Lim, E. P., and H. H. Hendon, 2015: Understanding and predicting the strong Southern Annular Mode and its impact on the record wet east Australian spring 2010. *Climate Dyn.*, **44**, 2807–2824, https://doi.org/10.1007/s00382-014-2400-5.

——, ——, D. Hudson, M. Zhao, L. Shi, O. Alves, and G. Young, 2016: Evaluation of the ACCESS-S1 hindcasts for prediction of Victorian seasonal rainfall. Bureau of Meteorology, accessed 6 June 2021, http://www.bom.gov.au/research/publications/researchreports/BRR-019.pdf.

——, and Coauthors, 2021: Why Australia was not wet during spring 2020 despite La Niña. *Sci. Rep.*, **11**, 18423, https://doi.org/10.1038/s41598-021-97690-w.

Maher, P., and S. C. Sherwood, 2016: Skill in simulating Australian precipitation at the tropical edge. *J. Climate*, **29**, 1477–1496, https://doi.org/10.1175/JCLI-D-15-0548.1.

Marshall, G. J., 2003: Trends in the southern annular mode from observations and reanalyses. *J. Climate*, **16**, 4134–4143, https://doi.org/10.1175/1520-0442(2003)016<4134:TITSAM>2.0.CO;2.

McIntosh, P. C., and H. H. Hendon, 2018: Understanding Rossby wave trains forced by the Indian Ocean Dipole. *Climate Dyn.*, **50**, 2783–2798, https://doi.org/10.1007/s00382-017-3771-1.

——, M. J. Pook, J. S. Risbey, S. N. Lisson, and M. Rebbeck, 2007: Seasonal climate forecasts for agriculture: Towards better understanding and value. *Field Crops Res.*, **104**, 130–138, https://doi.org/10.1016/j.fcr.2007.03.019.

——, J. S. Risbey, J. N. Brown, and M. J. Pook, 2012: Apparent and real sources of rainfall associated with a cutoff low. *CAWCR Res. Lett.*, **8**, 4–9, https://www.cawcr.gov.au/researchletters/CAWCR_Research_Letters_8.pdf.

McKenna, S., A. Santoso, A. Sen Gupta, A. S. Taschetto, and W. Cai, 2020: Indian Ocean Dipole in CMIP5 and CMIP6: Characteristics, biases, and links to ENSO. *Sci. Rep.*, **10**, 11500, https://doi.org/10.1038/s41598-020-68268-9.

McPhaden, M. J., S. E. Zebiak, and M. H. Glantz, 2006: ENSO as an integrating concept in Earth science. *Science*, **314**, 1740–1745, https://doi.org/10.1126/science.1132588.

Meneghini, B., I. Simmonds, and I. N. Smith, 2007: Association between Australian rainfall and the Southern Annular Mode. *Int. J. Climatol.*, **27**, 109–121, https://doi.org/10.1002/joc.1370.

Meyers, G., P. McIntosh, L. Pigot, and M. Pook, 2007: The years of El Niño, La Niña, and interactions with the tropical Indian Ocean. *J. Climate*, **20**, 2872–2880, https://doi.org/10.1175/JCLI4152.1.

Nieto, R., R. Castillo, and A. Drumond, 2014: The modulation of oceanic moisture transport by the hemispheric annular modes. *Front. Earth Sci.*, **2**, https://doi.org/10.3389/feart.2014.00011.

Pepler, A. S., A. J. Dowdy, and P. Hope, 2021: The differing role of weather systems in southern Australian rainfall between 1979–1996 and 1997–2015. *Climate Dyn.*, **56**, 2289–2302, https://doi.org/10.1007/s00382-020-05588-6.

Perkins, S. E., D. Argüeso, and C. J. White, 2015: Relationships between climate variability, soil moisture, and Australian heatwaves. *J. Geophys. Res. Atmos.*, **120**, 8144–8164, https://doi.org/10.1002/2015JD023592.

Pook, M., J. Risbey, and P. McIntosh, 2010: East coast lows, atmospheric blocking and rainfall: A Tasmanian perspective. *IOP Conf. Ser. Earth Environ. Sci.*, **11**, 012011, https://doi.org/10.1088/1755-1315/11/1/012011.

Pui, A., A. Sharma, A. Santoso, and S. Westra, 2012: Impact of the El Niño–Southern Oscillation, Indian Ocean dipole, and southern annular mode on daily to subdaily rainfall characteristics in East Australia. *Mon. Wea. Rev.*, **140**, 1665–1682, https://doi.org/10.1175/MWR-D-11-00238.1.

Rathore, S., N. L. Bindoff, C. C. Ummenhofer, H. E. Phillips, and M. Feng, 2020: Near-surface salinity reveals the oceanic sources of moisture for Australian precipitation through atmospheric moisture transport. *J. Climate*, **33**, 6707–6730, https://doi.org/10.1175/JCLI-D-19-0579.1.

Reid, K. J., I. Simmonds, C. L. Vincent, and A. D. King, 2019: The Australian northwest cloudband: Climatology, mechanisms, and association with precipitation. *J. Climate*, **32**, 6665–6684, https://doi.org/10.1175/JCLI-D-19-0031.1.

Risbey, J. S., M. J. Pook, P. C. McIntosh, M. C. Wheeler, and H. H. Hendon, 2009: On the remote drivers of rainfall variability in Australia. *Mon. Wea. Rev.*, **137**, 3233–3253, https://doi.org/10.1175/2009MWR2861.1.

Saji, N. H., B. N. Goswami, P. N. Vinayachandran, and T. Yamagata, 1999: A dipole mode in the tropical Indian Ocean. *Nature*, **401**, 360–363, https://doi.org/10.1038/43854.

Unauthenticated | Downloaded 01/24/24 02:40 AM UTC

——, T. Ambrizzi, and S. E. T. Ferraz, 2005: Indian Ocean Dipole mode events and austral surface air temperature anomalies. *Dyn. Atmos. Oceans*, **39**, 87–101, https://doi.org/10.1016/j.dynatmoce.2004.10.015.

Santoso, A., M. J. Mcphaden, and W. Cai, 2017: The defining characteristics of ENSO extremes and the strong 2015/2016 El Niño. *Rev. Geophys.*, **55**, 1079–1129, https://doi.org/10.1002/2017RG000560.

Sen Gupta, A., and M. H. England, 2006: Coupled ocean–atmosphere–ice response to variations in the southern annular mode. *J. Climate*, **19**, 4457–4486, https://doi.org/10.1175/JCLI3843.1.

Taschetto, A. S., A. Sen Gupta, N. C. Jourdain, A. Santoso, C. C. Ummenhofer, and M. H. England, 2014: Cold tongue and warm pool ENSO Events in CMIP5: Mean state and future projections. *J. Climate*, **27**, 2861–2885, https://doi.org/10.1175/JCLI-D-13-00437.1.

Thompson, D. W. J., and S. Solomon, 2002: Interpretation of recent Southern Hemisphere climate change. *Science*, **296**, 895–899, https://doi.org/10.1126/science.1069270.

Tozer, C. R., J. S. Risbey, T. J. O'Kane, D. P. Monselesan, and M. J. Pook, 2018: The relationship between wave trains in the Southern Hemisphere storm track and rainfall extremes over Tasmania. *Mon. Wea. Rev.*, **146**, 4201–4230, https://doi.org/10.1175/MWR-D-18-0135.1.

Ukkola, A. M., M. G. De Kauwe, M. L. Roderick, G. Abramowitz, and A. J. Pitman, 2020: Robust future changes in meteorological drought in CMIP6 projections despite uncertainty in precipitation. *Geophys. Res. Lett.*, **47**, e2020GL087820, https://doi.org/10.1029/2020GL087820.

Ummenhofer, C. C., M. H. England, P. C. McIntosh, G. A. Meyers, M. J. Pook, J. S. Risbey, A. Sen Gupta, and A. S. Taschetto, 2009: What causes southeast Australia's worst droughts? *Geophys. Res. Lett.*, **36**, L04706, https://doi.org/10.1029/2008GL036801.

——, and Coauthors, 2010: Indian and Pacific Ocean influences on southeast Australian drought and soil moisture. *J. Climate*, **24**, 1313–1336, https://doi.org/10.1175/2010JCLI3475.1.

——, P. C. McIntosh, M. J. Pook, and J. S. Risbey, 2013: Impact of surface forcing on Southern Hemisphere atmospheric blocking in the Australia–New Zealand sector. *J. Climate*, **26**, 8476–8494, https://doi.org/10.1175/JCLI-D-12-00860.1.

——, A. Sen Gupta, M. H. England, A. S. Taschetto, P. R. Briggs, and M. R. Raupach, 2015: How did ocean warming affect Australian rainfall extremes during the 2010/2011 La Niña event? *Geophys. Res. Lett.*, **42**, 9942–9951, https://doi.org/10.1002/2015GL065948.

van Rensch, P., A. J. E. Gallant, W. Cai, and N. Nicholls, 2015: Evidence of local sea surface temperatures overriding the southeast Australian rainfall response to the 1997–1998 El Niño. *Geophys. Res. Lett.*, **42**, 9449–9456, https://doi.org/10.1002/2015GL066319.

——, J. Arblaster, A. J. E. Gallant, W. Cai, N. Nicholls, and P. J. Durack, 2019: Mechanisms causing east Australian spring rainfall differences between three strong El Niño events. *Climate Dyn.*, **53**, 3641–3659, https://doi.org/10.1007/s00382-019-04732-1.

Verdon, D. C., and S. W. Franks, 2005: Indian Ocean sea surface temperature variability and winter rainfall: Eastern Australia. *Water Resour. Res.*, **41**, W09413, https://doi.org/10.1029/2004WR003845.

Weller, E., and W. Cai, 2013: Realism of the Indian Ocean dipole in CMIP5 models: The implications for climate projections. *J. Climate*, **26**, 6649–6659, https://doi.org/10.1175/JCLI-D-12-00807.1.

Unauthenticated | Downloaded 01/24/24 02:40 AM UTC